Crystal structure and catalytic mechanism of the essential m^{1}G37 tRNA methyltransferase TrmD from *Pseudomonas aeruginosa*

JUTHAMAS JAROENSUK,[1,2,11,13] YEE HWA WONG,[3,4,13] WENHE ZHONG,[2,4] CHONG WAI LIEW,[4] SOMCHART MAENPUEN,[5] ABBAS E. SAHILI,[3,4] SOPAPAN ATICHARTPONGKUL,[6] YOK HIAN CHIONH,[2,12] QIANHUI NAH,[2] NARUMON THONGDEE,[1] MEGAN E. MCBEE,[2] ERIN G. PRESTWICH,[7] MICHAEL S. DEMOTT,[7] PIMCHAI CHAIYEN,[8] SKORN MONGKOLSUK,[6,9,10] PETER C. DEDON,[2,7] JULIEN LESCAR,[3,4] and MAYUREE FUANGTHONG[1,6,10]

[1]Applied Biological Sciences Program, Chulabhorn Graduate Institute, Chulabhorn Royal Academy, Bangkok 10210, Thailand
[2]Singapore-MIT Alliance for Research and Technology Antimicrobial Resistance and Infectious Disease Interdisciplinary Research Groups, 138602 Singapore
[3]School of Biological Sciences, Nanyang Technological University, 637551 Singapore
[4]NTU Institute of Structural Biology, Nanyang Technological University, 636921 Singapore
[5]Department of Biochemistry, Faculty of Science, Burapha University, Chonburi 20131, Thailand
[6]Laboratory of Biotechnology, Chulabhorn Research Institute, Bangkok 10210, Thailand
[7]Department of Biological Engineering, Massachusetts Institute of Technology, Cambridge, Massachusetts 02139, USA
[8]School of Biomolecular Science and Engineering, Vidyasirimedhi Institute of Science and Technology (VISTEC), Rayong 21210, Thailand
[9]Department of Biotechnology, Faculty of Sciences, Mahidol University, Bangkok 10400, Thailand
[10]Center of Excellence on Environmental Health and Toxicology (EHT), Bangkok 10400, Thailand

ABSTRACT

The tRNA (m^{1}G37) methyltransferase TrmD catalyzes m^{1}G formation at position 37 in many tRNA isoacceptors and is essential in most bacteria, which positions it as a target for antibiotic development. In spite of its crucial role, little is known about TrmD in *Pseudomonas aeruginosa* (*Pa*TrmD), an important human pathogen. Here we present detailed structural, substrate, and kinetic properties of *Pa*TrmD. The mass spectrometric analysis confirmed the G36G37-containing tRNAs Leu(GAG), Leu(CAG), Leu(UAG), Pro(GGG), Pro(UGG), Pro(CGG), and His(GUG) as *Pa*TrmD substrates. Analysis of steady-state kinetics with *S*-adenosyl-L-methionine (SAM) and tRNA$^{Leu(GAG)}$ showed that *Pa*TrmD catalyzes the two-substrate reaction by way of a ternary complex, while isothermal titration calorimetry revealed that SAM and tRNA$^{Leu(GAG)}$ bind to *Pa*TrmD independently, each with a dissociation constant of 14 ± 3 µM. Inhibition by the SAM analog sinefungin was competitive with respect to SAM (K_i = 0.41 ± 0.07 µM) and uncompetitive for tRNA (K_i = 6.4 ± 0.8 µM). A set of crystal structures of the homodimeric *Pa*TrmD protein bound to SAM and sinefungin provide the molecular basis for enzyme competitive inhibition and identify the location of the bound divalent ion. These results provide insights into *Pa*TrmD as a potential target for the development of antibiotics.

Keywords: *Pseudomonas*; TrmD; tRNA modification; tRNA (m1G37) methyltransferase

INTRODUCTION

Pseudomonas aeruginosa infection has become a serious global public health threat (Lucena et al. 2014; Hong et al. 2015; Ventola 2015), due in part to increasing resistance to antibiotics such as carbapenems (National Nosocomial Infections Surveillance System 2004; Centers for Disease Control Ministry of Health and Welfare R.O.C. Taiwan 2010). This has fostered efforts to discover novel

[11]**Present address:** School of Biomolecular Science and Engineering, Vidyasirimedhi Institute of Science and Technology (VISTEC), Rayong 21210, Thailand.
[12]**Present address:** Tychan Ltd., 117604 Singapore.
[13]These authors contributed equally to this work.
Corresponding authors: mayuree@cri.or.th, julien@ntu.edu.sg, pcdedon@mit.edu
Article is online at http://www.rnajournal.org/cgi/doi/10.1261/rna.066746.118.

targets for antibiotic development, including tRNA-modifying enzymes. In all organisms, tRNA is transcribed as a pre-tRNA that is processed to maturity by a variety of editing steps such as CCA addition and by extensive posttranscriptional chemical modification of the four canonical ribonucleotides (El Yacoubi et al. 2012). While these modifications are widely distributed throughout the tRNA molecule and affect ~10% of the ~80–90 tRNA nucleotides, modifications at positions 32, 34, and 37 are recognized for their role in regulating cellular stress responses (Begley et al. 2007; Chan et al. 2012; Chionh et al. 2016; Jaroensuk et al. 2016) and promoting antibiotic resistance (Taylor et al. 1998). In this regard, the tRNA (m^1G37) methyltransferase TrmD (Byström and Björk 1982; Hjalmarsson et al. 1983; Hou et al. 2017), which is essential in most bacterial species (Hagervall et al. 1993; Forsyth et al. 2002; Björk and Nilsson 2003; O'Dwyer et al. 2004; de Berardinis et al. 2008; Winsor et al. 2011), has emerged as an important target for drug development (Lahoud et al. 2011; Hill et al. 2013; Baumgartner and Camacho 2016). TrmD uses *S*-adenosylmethionine (SAM) as a methyl donor and catalyzes the methylation of G37 to form 1-methylguanosine (m^1G) mainly in tRNAs containing a G36G37 motif, thus reading codons that start with C, including those for leucine (CUN), proline (CCN), and arginine (CCG) (Björk et al. 2001; Sprinzl and Vassilenko 2005). Only TrmD from *Aquifex aeolicus* is known to recognize tRNAs with A36G37 (Takeda et al. 2006). With a general requirement for Mg^{2+} to promote proton abstraction from N1 of G37 and stabilize the negative charge on O^6 of G37 (Sakaguchi et al. 2014; Ito et al. 2015), structural analysis of TrmD from *Escherichia coli* and *Haemophilus influenzae* revealed a homodimer that uses a deep trefoil knot structure at its amino-terminal domain for SAM binding (Elkins et al. 2003; Ito et al. 2015), in contrast to the human homolog, Trm5, which is active in a monomeric form and uses a Rossmann fold for SAM (Goto-Ito et al. 2008). The presence of m^1G37 has been shown to be essential for maintaining the ribosome reading-frame and fidelity of protein synthesis (Björk et al. 1989), with its loss leading to increased +1 frameshifting events, premature termination of protein translation, and cellular toxicity (Björk et al. 1989; Hagervall et al. 1993; Li and Björk 1995). While well studied in a variety of bacteria, the structure and properties of TrmD in *P. aeruginosa* have not been reported.

Here we establish that the *PA14_15990* gene in *P. aeruginosa* PA14 is a TrmD m^1G37-forming tRNA methyltransferase, and characterize its structure, kinetics and substrate properties. The results revealed that *Pa*TrmD catalyzes the formation of m^1G37 in tRNA by a ternary complex mechanism in which tRNA and SAM can bind the protein independently. The unique and shared features of *Pa*TrmD presented here expand the opportunities for developing TrmD as an antibiotic target.

RESULTS AND DISCUSSION

PA14_15990 (trmD) is essential for growth in *P. aeruginosa* PA14

Attempts to construct a *PA14_15990/trmD* mutant in *P. aeruginosa* PA14 using homologous recombination were not successful, which is consistent with reports that *trmD* is essential in *E. coli*, *Streptococcus pneumoniae*, and *Staphylococcus aureus* (O'Dwyer et al. 2004; Chaudhuri et al. 2009). We therefore tested the essentiality of *PA14_15990/trmD* in *P. aeruginosa* PA14 using a temperature-sensitive allele of a *Pseudomonas* replicon, mSF*ts*[1] (Silo-Suh et al. 2009), to regulate expression of extra chromosomal *trmD*. Wild-type (WT) *P. aeruginosa* PA14 containing pBBR-*trmD*-mSF^{ts1} and the *trmD* conditional knockout strain (*trmD*::Gm/pBBR-*trmD*-mSF^{ts1}) were both grown at a permissive temperature to maintain the stability of the plasmid (28°C and 37°C) or at a nonpermissive temperature to cause plasmid loss (46°C). As demonstrated in Figure 1, the growth of the *trmD* conditional knockout strain at the permissive temperature was similar to WT PA14 (Fig. 1A,B), while growth of the knockout strain was no longer observed at the nonpermissive temperature (Fig. 1C). These results suggest that *Pa*TrmD is essential in *P. aeruginosa* PA14.

PA14_15990 encodes a tRNA (m^1G37) methyltransferase homolog

Homology analyses (BLASTp) using *E. coli* TrmD (*Ec*TrmD) to search against the *P. aeruginosa* PA14 genome resulted in one hit with PA14_15990 sharing 66% identity to *Ec*TrmD. As shown in Figure 2A, a protein sequence alignment of PA14_15990 and TrmD homologs with known structures from *Haemophilus influenza* (*Hi*TrmD) (Ahn et al. 2003), *Aquifex aeolicus* (*Aa*TrmD) (Liu et al. 2003), and *E. coli* (Elkins et al. 2003), reveals that *Pa*TrmD has 64% amino acid identity with the *Hi*TrmD and 41% amino acid identity with the *Aa*TrmD. *Pa*TrmD also shares functionally important amino acid residues involved in cofactor binding (Ser93–Gly96, Gly118, Ile123, Ser137, Gly145), tRNA binding (Gly60, Gly64, Ser203–His206), and catalytic activity (Asp54, Arg159, and Asp174). These results support the idea that *PA14_15990* encodes the tRNA (m^1G37) methyltransferase (TrmD) in *P. aeruginosa* PA14. Subsequent structural, biochemical and kinetic data support this conclusion.

The overall structure of *Pa*TrmD

The structure of the *Pa*TrmD protein bound to the copurified methyl donor SAM was determined at a resolution of 2.16 Å. A schematic representation of the topology of the *Pa*TrmD monomer and of its fold is shown in Figure 2B,C.

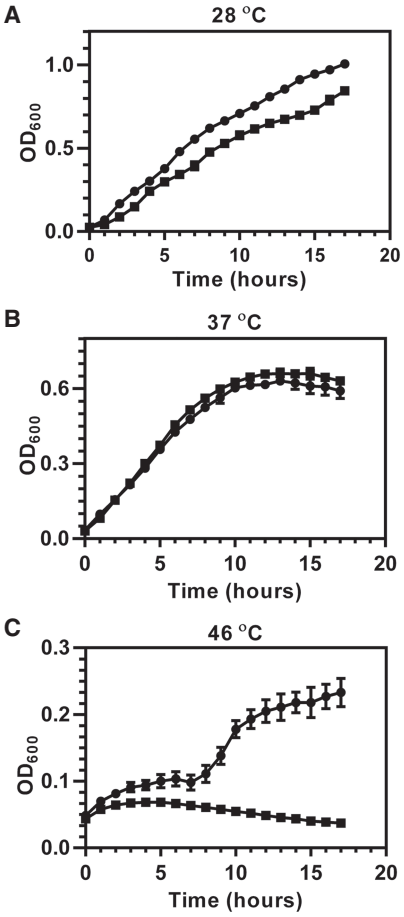

FIGURE 1. Growth of wild-type *P. aeruginosa* PA14 and the *trmD* conditional knockout strain establishes TrmD as an essential enzyme in PA14. Wild-type PA14 (-●-) and the *trmD* conditional knockout strain (-■-) were grown in LB broth in 96-well plates, and growth was monitored for 18 h at temperatures that maintain stability of the plasmid carrying *trmD* gene (*A*, 28°C; *B*, 37°C) or cause loss of the plasmid (*C*, 46°C).

A second crystal structure of *Pa*TrmD bound to the SAM-competitive inhibitor sinefungin (SFG) was refined at a resolution of 2.45 Å. In order to unambiguously locate the divalent ion, a third structure where crystals of *Pa*TrmD were soaked with Mn^{2+} and SFG was determined (Table 1). For these three structures, the refined model comprises a homodimer in the asymmetric unit with the two monomers (Fig. 2B,C; Supplemental Fig. S1) related by a non-crystallographic dyad (Fig. 2D). Pairwise comparisons with published TrmD structures from *E. coli* (PDB code 1P9P) (Elkins et al. 2003), *H. influenzae* (PDB code 1UAK) (Ahn et al. 2003), and *A. aeolicus* (PDB code 1OY5) (Liu et al. 2003) return deviation values of 0.9, 1.0, and 2.4 Å for 235, 236, and 205 superimposed α-carbons, respectively. A structure-based sequence alignment of TrmD from nine bacteria is displayed in Supplemental Figure S2. The active site is located in a pocket of the trefoil knot at the dimer interface (Supplemental Fig. S1). The *Pa*TrmD monomer is formed by an amino-terminal domain (NTD) that adopts an α/β fold (residues 5–165) and a mostly helical carboxy-terminal domain (CTD) spanning residues 178-250 (Fig. 2B,C). These two domains are connected by a linker spanning residues 166–177 that acts as a lid covering up the active site (Fig. 2; Supplemental Fig. S1). The lid was reported to become ordered only upon tRNA binding, which is accompanied by folding into an α-helix (Ito et al. 2015). Here, the lid appears rather flexible in the two molecules present in the asymmetric unit of the SAM complex and more ordered in the complexes with SFG. Thus, in the SAM-bound structure, residues 166–173 are missing from the model and for the SFG complexes, residues 167–172 are missing in molecule A while the loop could be built entirely for molecule B (Fig. 3A,B; Supplemental Fig. S4).

Features of *Pa*TrmD bound to SAM and SFG

Clear electron density corresponding to two bound SAM molecules per *Pa*TrmD dimer was visible (Fig. 3B; Supplemental Fig. S4). SAM adopts a bent conformation with the adenine moiety in an *anti* conformation and the ribose pucker in C3′-endo (Fig. 3B). Since no SAM was added during purification and crystallization, it presumably originates from the *E. coli* culture medium and has copurified with the protein. The adenine base is stacked between Pro94 and Pro149. Its N^6 atom hydrogen bonds with carbonyl oxygen atoms of Gly139 and Tyr141, while the 2′-hydroxyl group of the ribose hydrogen bonds with the carbonyl oxygen of Leu92 and the amide group of Gly118 (Fig. 3B; Supplemental Fig. S4). The 3′-hydroxyl group of the ribose forms another hydrogen bond with the side chain of Tyr91. The amino acid tail of SAM is stabilized by two sets of polar interactions: (i) the side chains of Gln95 and His185* (residues from chain B are marked by an asterisk) make contact with the carboxylic group of SAM and (ii) the amino tail makes a salt bridge with the carboxylic group of residues Asp182* (Fig. 3B; Supplemental Fig. S4).

SFG is an isosteric analog of SAM, in which the methyl group of SAM is replaced by an amino group and the sulfur by a carbon atom. The protein components of the SFG- and SAM-bound structures are closely superimposable, with an RMS deviation of 0.58 Å for all 252 C_α atoms. However, a close-up view of the superposed active sites reveals conformational changes at the level of the amino acid tails of the ligands (Fig. 3A; Supplemental Fig. S5). The carboxylic group of SFG is reoriented toward the interdomain linker, forming a close hydrogen bond with Ser175*, while its amino group hydrogen bonds the side chain of Asp182*. These additional contacts account for the lid ordering in the SFG complex compared to the SAM complex.

Given the need for an Mg^{2+} ion for catalysis, our search of the electron density map revealed a possible location for

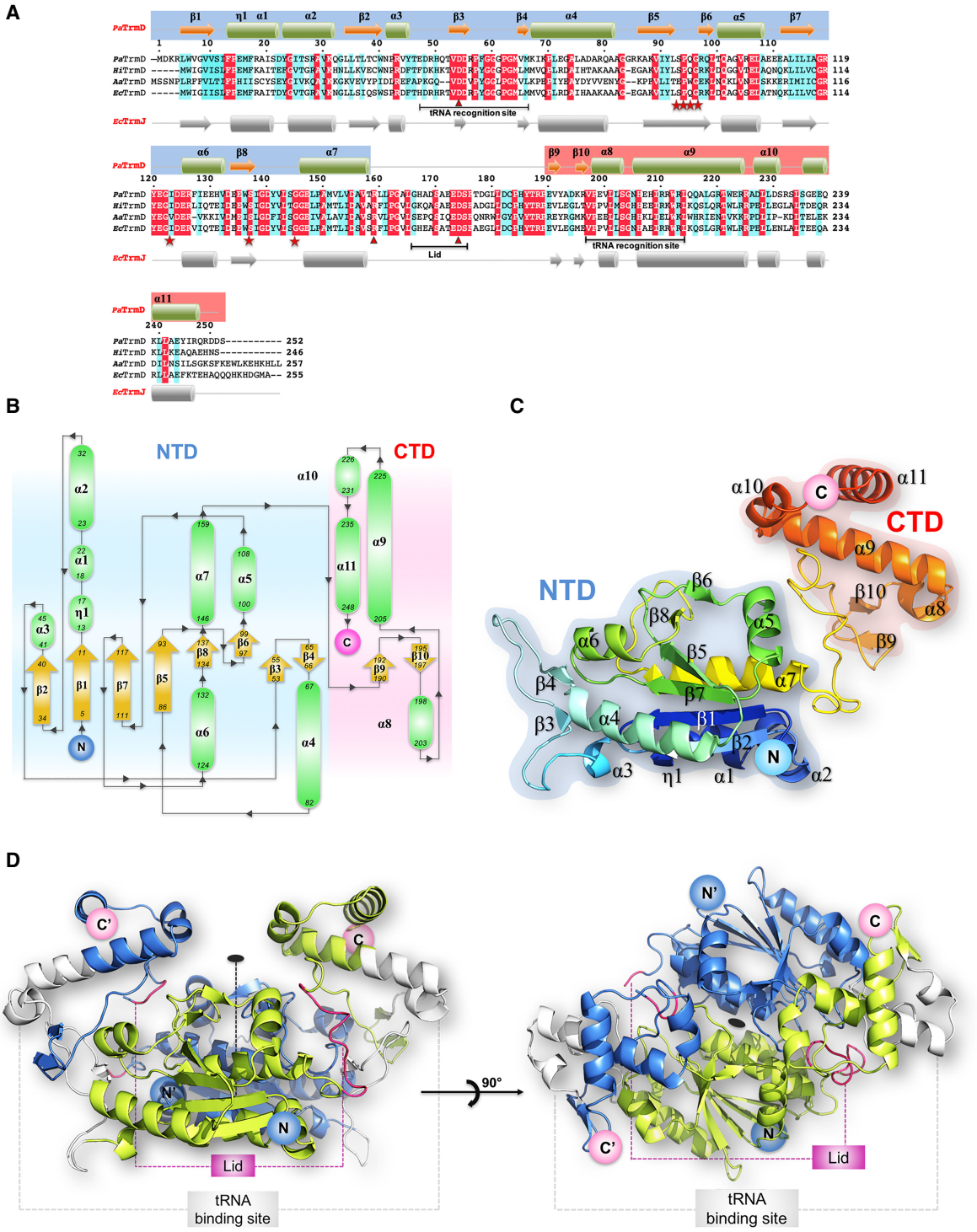

FIGURE 2. The structure of *Pa*TrmD. (*A*) Structure-based sequence alignment showing the amino acid sequences of TrmD from *P. aeruginosa* PA14 (*Pa*TrmD, this work), *H. influenzae* (*Hi*TrmD), *A. aeolicus* (*Aa*TrmD), and *E. coli* (*Ec*TrmD). The amino acids involved in cofactor binding are indicated by stars in red, and amino acids involved in the catalytic activity are indicated by triangles. (*B*) Schematic representation of the *Pa*TrmD monomer topology (with the NTD shaded in blue and the CTD in pink) indicating the arrangement of secondary structure elements (α-helices are represented as green ovals and β-strands as yellow arrows) with the residues numbered. The amino and carboxyl termini are indicated. (*C*) Model representation of the *Pa*TrmD monomer 3D structure colored from dark blue (amino terminus) to red (carboxyl terminus). (*D*) Overall view of the *Pa*TrmD homodimer present in the asymmetric unit (one monomer is colored blue and the other light green). The dyad in the plane of the figure is represented by a dashed line and by an oval (perpendicular to the plane of the figure) in the *right* panel. Main functional elements are indicated: lid (or interdomain linker region) and the possible tRNA binding sites (one being used at a time yielding a 2:1 stoichiometry) (Ito et al. 2015).

TABLE 1. Crystallographic data and refinement statistics

PDB code	*Pa*TrmD-SAM 5WYQ	*Pa*TrmD-sinefungin 5WYR	*Pa*TrmD- sinefungin-Mn 6JKI
Data collection			
Resolution range (Å)	28.12–2.16 (2.29–2.16)	42.65–2.45 (2.56–2.45)	50.00–2.60 (2.59–2.60)
Beamline	X06DA, SLS	X06DA, SLS	Proxima-2A, SOLEIL
Space group	$P3_221$	$P3_221$	$P3_221$
Dimers per asymmetric unit	1	1	1
Cell parameters: *a*,*b*,*c* (Å); α,β,γ (°)	85.90, 85.90, 147.84; 90, 90, 120	85.29, 85.29, 147.84; 90, 90, 120	85.68, 85.68, 147.61; 90, 90, 120
No. of measured reflections	120,767 (10,006)	123,092 (14,245)	739,353 (116,722)
No. of unique reflections	34,505 (2,943)	23,225 (2,638)	37,629 (6,010)
Completeness (%)	99.9 (99.9)	99.3 (99.4)	99.8 (98.9)
Multiplicity	3.5	5.3	19.6
R_{merge}[a]	0.057 (0.910)	0.088 (0.741)	0.187 (1.374)
$CC_{1/2}$[b]	0.99 (0.88)	0.99 (0.91)	0.99 (0.88)
Average $I/\sigma(I)$	15.9 (1.7)	16.9 (3.1)	14.38 (1.85)
Refinement			
Resolution range (Å)	28.12–2.16 (2.23–2.16)	40.96–2.45 (2.56–2.45)	26.16–2.59 (2.73–2.59)
R factor (R_{work}[c]/R_{free}[d]) (%)	20.7/24.9	19.1/23.1	20.7/24.5
Model contents			
Protein atoms	3804	3875	3848
Water molecules	180	161	121
Ligand atoms	54 (2 × SAM)	54 (2 × SFG)	54 (2 × SFG) 14 (2 × PEG) 30 (5 × GOL) (2 × Na) (3 × Mn)
Root mean square deviation			
Distances (Å)	0.010	0.010	0.010
Bond angles (°)	1.02	1.08	1.18
Clash score	3.69	6.99	3.95
Rotamer outliers (%)	0.75	0.25	0.75
Ramachandran plot			
Favored (%)	96.8	96.7	97.91
Allowed (%)	3.2	3.3	2.09
Outlier (%)	0	0	0

Values in parentheses indicate values in the highest resolution shell.
[a] $R_{merge} = \sum|I_j - \langle I \rangle|/\sum I_j$, where I_j is the intensity of an individual reflection and is the average intensity of that reflection.
[b] $CC_{1/2}$ = percentage of correlation between intensities from random half-data set.
[c] $R_{work} = \sum||F_o| - |F_c||/\sum|F_c|$, where F_o denotes the observed structure factor amplitude, and F_c the structure factor amplitude calculated from the model.
[d] R_{free} is as for R_{work} but calculated with 5% of randomly chosen reflections omitted from the refinement.

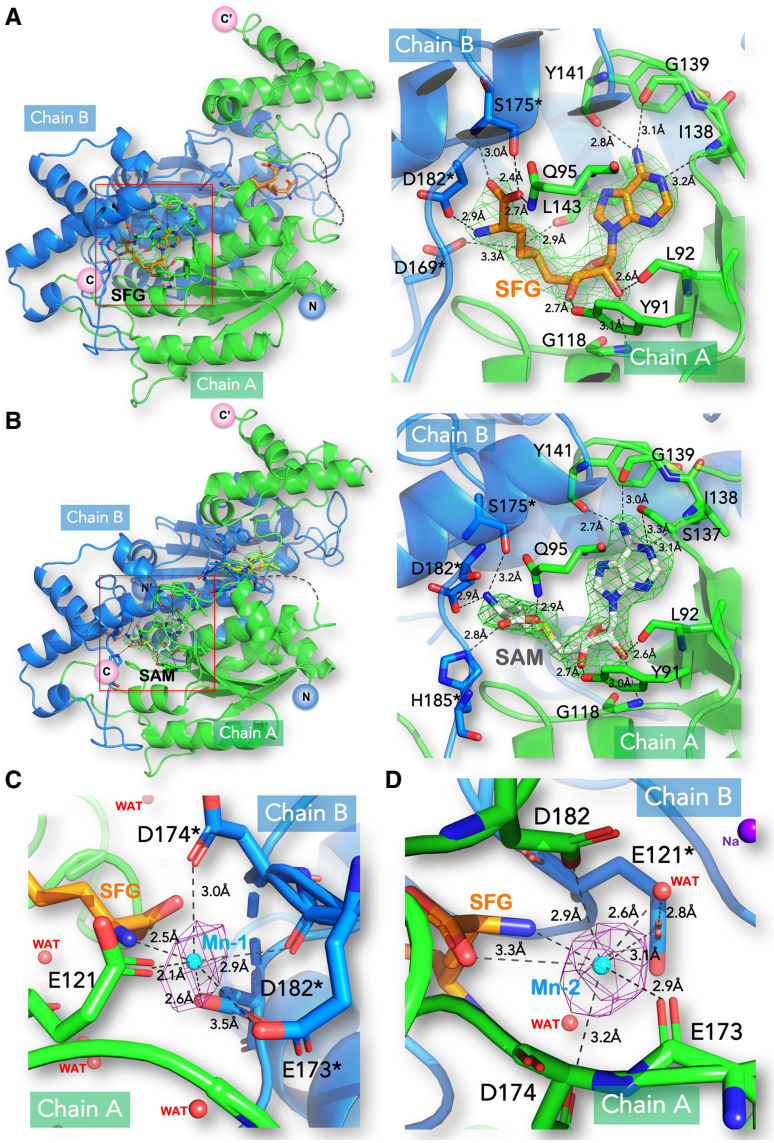

FIGURE 3. Structures of the *Pa*TrmD-SFG, *Pa*TrmD-SAM, and *Pa*TrmD-SFG-Mn complexes. (*A*,*B*) Overall (*left* panels) and magnified views (*right* panels) for the two binary complexes of TrmD with sinefungin (SFG) (*A*) and SAM (*B*). Subunits A and B of the TrmD homodimer are colored green and blue, respectively. Residues from chain B are marked by an asterisk. The SFG ligand is depicted as orange sticks and SAM as white sticks. Polar contacts are represented by dashed lines with interacting residues labeled and ligand-protein distances in Å. Difference Fourier electron density maps where the bound ligands were omitted from the model for phase calculation are overlaid and contoured at a level of 3σ; simulated annealing is shown in Supplemental Figure S3. (*C*,*D*) The *Pa*TrmD-SFG-Mn complex. The anomalous electron density map allowing unambiguous positioning of the bound manganese in the active site (Mn) in the presence of SFG (see Supplemental Fig. S8 for the measurement of the *K* absorption edge of Mn in the crystal). The anomalous map (colored in purple) was calculated from 40 to 5 Å and contoured at a level of 4.6 σ. Mn is coordinated by a side-chain carbonyl group of E173*, carboxylic groups of E121, D174*, and D182*, and the nitrogen atom of the SFG tail. These interacting residues and the ligand SFG are shown as sticks. Mn is shown as a cyan sphere.

such a divalent ion. We found hints for the presence of an Mg^{2+} ion in the active site near the carboxylic tail of SAM. However, the octahedral coordination shell was incomplete and the putative position did not match the location of Mn^{2+} (for the SFG-Mn^{2+} complex) that we could confidently assign based on a clear anomalous signal (see below). Next, we measured the Mg^{2+} content in the *Pa*TrmD protein and found that the molar ratios of *Pa*TrmD to Mg^{2+} ion of the Mg^{2+}-reconstituted *Pa*TrmD was 1:0.97 (Table 2). These data imply that one *Pa*TrmD monomer can bind to one Mg^{2+} ion. Conversely, the molar ratio of *Pa*TrmD to Mg^{2+} ion for the purified enzyme without the Mg^{2+} reconstitution was 1:0.02 indicating that Mg^{2+} ion does not bind tightly to *Pa*TrmD. This is consistent with the reported weak Mg^{2+} binding affinity for *E. coli* TrmD of 0.7 mM, (Sakaguchi et al. 2014). We then investigated the presence of a bound divalent metal at the active site: We soaked *Pa*TrmD crystals with manganese (Mn^{2+}) and sinefungin (SFG) and collected these data at the Mn^{2+} K edge to maximize the anomalous signal (see Materials and Methods). In Figure 3C,D, two peaks in the anomalous Fourier map were readily apparent at >5 sigma level. One Mn^{+2} near each of the bound SFG could be built. Mn^{+2} is coordinated by a side-chain carbonyl group of E173*, carboxylic groups of E121, D174*, and D182*, and the nitrogen atom of the SFG tail (Fig. 3C,D). Although the catalytic mechanism that was proposed for the majority of SAM-dependent methyl transferases requires no divalent metal ions, Sakaguchi et al. reported that TrmD-catalyzed methyl transfer from SAM to the N^1 atom of G37 from the tRNA is strongly dependent on the presence of divalent metal ions, with Mg^{2+} as the most physiologically relevant (Sakaguchi et al. 2014; Hou et al. 2017). Based on the pH-activity profile, they proposed a catalytic mechanism in which Mg^{2+} increases the nucleophilicity of N^1 of G37 and stabilizes the developing negative charge on O^6 during an attack on the methyl sulfonium of the SAM donor. Moreover, an Mg^{2+} ion was also found near the active site in contact with the N^7 atom of G37 in a ternary complex between TrmD from *H. influenzae*, tRNA and SAM (Ito et al. 2015), lending further

TABLE 2. Measurement of Mg^{2+} using ICP-OES

Sample	Concentration of *Pa*TrmD	Concentration of Mg^{2+}	TrmD:Mg^{2+} ratio
Reagent blank	Not applicable	0.730 ± 0.0257 μM	Not applicable
Purified *Pa*TrmD	20 μM	0.402 ± 0.0054 μM	1: 0.02
Purified *Pa*TrmD preincubated with 1 mM Mg_2Cl	20 μM	19.34 ± 0.114 μM	1: 0.97

The data represent mean ± SD for three independent determinations.

support for a positive contribution of Mg^{2+} ion to the catalytic mechanism. Interestingly, a requirement for a bent conformation of the methyl donor was proposed based on molecular dynamics simulations (Christian et al. 2016).

Conformational changes are required to form a ternary complex with tRNA

A TrmD enzymatic mechanism involving deprotonation of G37 by a catalytic base followed by a nucleophilic attack on the methyl group of SAM by the N1 atom has been proposed (Ahn et al. 2003; Elkins et al. 2003; Ito et al. 2015). The side chains of Arg159*, Leu165*, and Ser170* of *Pa*TrmD (Fig. 4) are well-positioned to form hydrogen bonds or to stack with G37, and Asp174* is the likely catalytic base (Figs. 2A, 4). Interestingly, Asp174* makes a salt bridge with Arg159*, in a conformation that might mimic a preactivated state in which the linker/lid is brought into proximity with the rest of the active site upon tRNA binding.

*Pa*TrmD catalyzes only the m^1G modification in PA14 tRNAs that possess a G36G37 motif

TrmD from most bacteria catalyzes the methylation m^1G37 in tRNAs containing a G36G37 motif (Björk et al. 2001; Sprinzl and Vassilenko 2005). Many conserved residues of *Pa*TrmD interact with G37 as mentioned above. In addition, the carboxylic group of an evolutionarily conserved Asp residue (Asp54 in *Pa*TrmD) interacts with the H atoms at positions N^1 and N^2 of G36 (Fig. 4C). A study in *E. coli* showed that *Ec*TrmD recognizes G36 as well as A36 with comparable binding affinity as the carboxylic groups of Asp54 interact with the hydrogen at position N^6 of A36 (Ito et al. 2015). However, the A36G37 sequence is not observed in bacterial tRNA. Here we tested whether the G36G37 motif is a substrate of *Pa*TrmD by defining the activity of *Pa*TrmD as a tRNA (m^1G37) methyltransferase by quantifying m^1G following in vitro reactions with synthetic PA14 tRNAs possessing a G36G37 motif, which are $tRNA^{Leu(CAG)}$, $tRNA^{Leu(UAG)}$, $tRNA^{His(GUG)}$, $tRNA^{Pro(GGG)}$, $tRNA^{Pro(CGG)}$, and $tRNA^{Pro(UGG)}$. $tRNA^{Gln(UUG)}$ with a G36A37 dinucleotide served as a negative control. Analysis of the 23 ribonucleosides shown in Supplemental Table S2 by HPLC-coupled tandem quadrupole mass spectrometry (LC-MS/MS) relative to standards revealed only a single modification, m^1G, in all G36G37-containing tRNAs (Fig. 5A). This is illustrated in the extracted ion chromatogram for $tRNA^{Pro(GGG)}$ shown in Figure 5B. As expected, m^1G was not detected in the G36A37-containing $tRNA^{Gln(UUG)}$. The fact that *Pa*TrmD catalyzes m^1G formation in synthetic tRNA substrates indicates that *Pa*TrmD can use G36G37-containing tRNAs without other modifications as substrates. Initially, the TrmD-mediated m^1G37 modification was shown for a subset of $tRNA^{Leu}$, $tRNA^{Pro}$, and $tRNA^{Arg}$ in bacteria (Li and Björk 1999; Ito et al. 2015). With genome sequencing analyses additional tRNA substrates for TrmD are predicted (Subramanian et al. 2014; Chan and Lowe 2016). In this study, our data expand the substrate specificity of TrmD from $tRNA^{Leu}$, $tRNA^{Pro}$, and $tRNA^{Arg}$ to $tRNA^{His}$ in bacteria. The substrate specificity is driven by the presence of G36G37 in each species.

*Pa*TrmD catalyzes m^1G at position 37 in the tRNA anticodon loop

Having established the m^1G product of *Pa*TrmD activity, we next defined the position of the m^1G in tRNAs by mass spectrometry-based RNA fragment analysis. Methylated $tRNA^{Leu(GAG)}$ from an in vitro reaction with *Pa*TrmD was digested with RNase A to give a signature oligoribonucleotide, $GAGm^1GU$, carrying m^1G at position 37. As shown in Figure 5C,D, the doubly charged negative ion (*m/z* 810.1356) of fragment $GAGm^1GU$ was observed at an HPLC retention time of 18.9 min. To determine the position of m^1G, the doubly charged ion *m/z* 810.1356 was analyzed by CID, with product ions shown in Figure 5E. The resulting CID mass spectra were analyzed with Simple Oligonucleotide Sequencer (SOS) (Rozenski and McCloskey 2002), with the ribonucleotide sequence determined based on the a-B-, w-, and y-ions. This analysis revealed that *Pa*TrmD catalyzes methyl transfer to G37 in the tRNA anticodon loop. This is entirely consistent with previous studies of *Ec*TrmD and *Hi*TrmD, in which TrmD was found to recognize and methylate tRNA substrates by making a contact with the D-arm, anticodon arm, and the variable region of tRNA (Ahn et al. 2003; Ito et al. 2015). The study of *Hi*TrmD demonstrated that TrmD uses the following conserved amino acid residues, Ser198, Gly199, His200/Asp200, and His201 of carboxy-terminal domain (CTD) to make contact with G37 in the substrate tRNAs for methylation (Ito et al. 2015). The structural and biochemical studies to this point prove that *Pa*TrmD catalyzes m^1G formation at position 37 in tRNAs

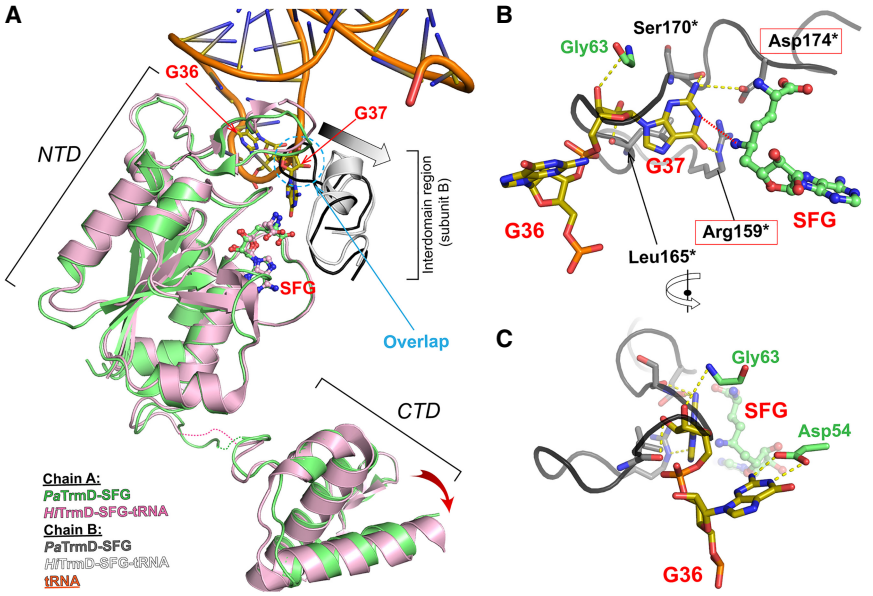

FIGURE 4. Comparison between the binary complex *Pa*TrmD-SFG and the ternary complex *Hi*TrmD-SFG/tRNA. Models of SFG-bound *Pa*TrmD (this work) and SFG/tRNA-bound *H. influenzae* TrmD (PDB ID: 4YVI) (Ito et al. 2015). The two complexes were superimposed based on the Cα atoms of NTD of subunit A. The interdomain region of subunit B is also displayed colored in dark gray (SFG-bound) or white (SFG/tRNA-bound), respectively. Ligands and key contacting residues are shown as sticks. Panel *A* highlights conformational differences; the interdomain region (subunit B, dark gray) of *Pa*TrmD-SFG would sterically collide with G37 of the bound tRNA in the ternary complex (dashed circle). Thus, a loop rearrangement is induced upon tRNA binding. The induced movement of the interdomain region (subunit B) is indicated by a gray arrow. The accompanying movement in CTD domain (subunit A) is shown by a red arrow. The poorly structured interdomain loops of subunit A are shown as dotted lines. (*B*,*C*) Orthogonal views of superposed structures showing the putative tRNA binding mode with *Pa*TrmD based on the experimental *Hi*TrmD-SFG/tRNA complex (Ito et al. 2015), highlighting the conservation of residues interacting with G37 between *Pa*TrmD and *Hi*TrmD. G37-interacting catalytic residues are in red boxes. The transfer of the methyl group to G37 is indicated by a red dotted line. Residues from chain B are marked by an asterisk. *Hi*TrmD structure was omitted for clarity.

containing a G36G37 motif. However, these studies do not provide insights into the enzymatic mechanism governing *Pa*TrmD activity. This was addressed next.

Steady-state kinetics of *Pa*TrmD

To gain insight into the kinetics and thermodynamics of *Pa*TrmD activity, we performed a series of enzymological and biophysical studies, starting with a detailed analysis of *Pa*TrmD kinetics. The linear range of the initial velocity of the methyltransferase reaction was first established by plotting initial velocities as a function of *Pa*TrmD concentration, which revealed linearity up to 36 nM (Supplemental Fig. S6). Working in this linear range, we investigated the steady-state kinetics of *Pa*TrmD by varying the concentrations of SAM and $tRNA^{Leu(GAG)}$ in reactions containing 23 nM *Pa*TrmD. The initial velocities were calculated and fit to the ternary complex Equation 1. A summary of steady-state kinetic parameters for *Pa*TrmD is shown in Table 3. The K_m of *Pa*TrmD for $tRNA^{Leu(GAG)}$ of 0.8 ± 0.2 μM is ~3- to 10-times smaller than that for *Ec*TrmD with $tRNA^{Pro(UAG)}$ (2.8 ± 0.1 μM) (Christian and Hou 2007), *Streptococcus pseumoniae* TrmD (*Sp*TrmD) with $tRNA^{Leu(CAG)}$ (4.3 ± 1.7 μM) (O'Dwyer et al. 2004), and *Hi*TrmD with $tRNA^{Leu(CAG)}$ (8.0 ± 1.1 μM) (Ito et al. 2015). The K_m of *Pa*TrmD for SAM was found to be 3.0 ± 0.8 μM, which is similar to data reported for *Ec*TrmD (5.0 ± 0.8 μM) (Lahoud et al. 2011) and *Hi*TrmD (3.0 μM) (Ito et al. 2015). *Pa*TrmD catalyzed the formation of m^1G with a K_{cat} of 13.0 ± 1.4 min^{-1}, which was comparable to values reported for *Hi*TrmD (19 ± 0.01 min^{-1}) (Ito et al. 2015) and *Sp*TrmD (15 ± 2 min^{-1}) (O'Dwyer et al. 2004). Overall, the kinetic properties of *Pa*TrmD quantified using the MTase-Glo assay are similar to other bacterial TrmD proteins previously characterized with a radiometric assay (Redlak et al. 1997; Brulé et al. 2004; O'Dwyer et al. 2004; Ito et al. 2015). When a double-reciprocal plot of $1/v_i$ versus 1/[SAM] at different fixed concentrations of the tRNA Leu^{GAG} was performed, the lines intersect (Fig. 6), which suggests that *Pa*TrmD operates by forming a ternary complex. This is consistent with previous analyses performed with TrmD from *S. pneumoniae* (O'Dwyer et al. 2004), *E. coli* (Redlak et al. 1997; Brulé et al. 2004) and *H. influenzae* (Ito et al. 2015; Christian et al. 2016). These results are also consistent with the structural data that revealed two separate binding pockets for tRNA and SAM (Figs. 2, 3) and with the ligand-binding analyses performed next.

SAM and tRNA bind to *Pa*TrmD independently

Since the kinetics studies suggested that methylation of G37 by *Pa*TrmD occurs in a ternary complex mechanism, we next investigated the interdependence of SAM and tRNA binding to *Pa*TrmD. Here we used isothermal titration calorimetry (ITC) to quantify binding of SAM and tRNA. $tRNA^{Leu(GAG)}$ was chosen as the substrate given its activity in the kinetics studies and the established position of the *Pa*TrmD-induced m^1G. Refolded *Pa*TrmD protein (Supplemental Fig. S7) was used here to eliminate the effects of copurified SAM.

As shown in Figure 7, our results suggest that SAM and tRNA can independently bind *Pa*TrmD to form the binary complexes *Pa*TrmD:SAM and *Pa*TrmD:tRNA. This is

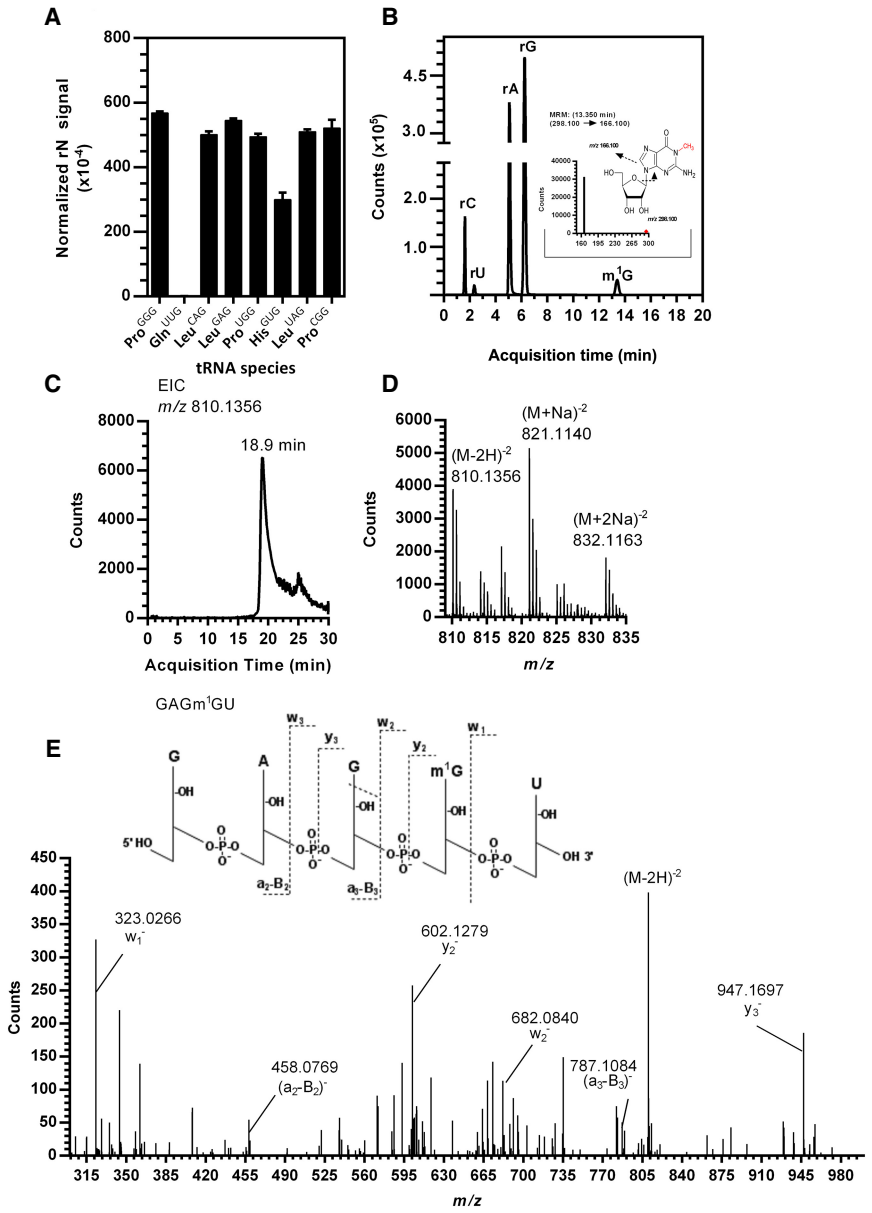

FIGURE 5. Quantification and mapping of m^1G catalyzed by *Pa*TrmD in synthetic $tRNA^{Leu(GAG)}$. (*A*) The level of m^1G in tRNAs reacted with *Pa*TrmD, and SAM was measured by HPLC-coupled triple-quadrupole mass spectrometry in tRNAs possessing G36G37 motifs and $tRNA^{Gln(UUG)}$ with a G36A37 motif. Values represent mean ± SD for three biological replicates. All ribonucleosides analyzed are shown in Supplemental Table S2. (*B*) Extracted ion chromatograms of ribonucleosides detected in *Pa*TrmD-methylated tRNA by LC-MS/MS in MRM mode. The *inset* shows the product ions arising from CID of the *m/z* 298.1 for parent m^1G. (*C*) Extracted ion chromatogram for *m/z* 810.1356 released from $tRNA^{Leu(GAG)}$ by RNase A and eluting at 18.9 min. (*D*) The mass spectrum for the $tRNA^{Leu(GAG)}$ oligo shows an $[M-2H]^{-2}$ ion with *m/z* 810.1356 and sodium adducts at *m/z* 821.1140 and 832.1163. (*E*) CID of *m/z* 810.1356 yields products consistent with $GAGm^1GU$.

consistent with previous analyses performed with TrmD from *S. pneumonia*, *E. coli* (Redlak et al. 1997; Brulé et al. 2004) and *H. influenzae* (Ito et al. 2015; Christian et al. 2016). Fitting the data for SAM and $tRNA^{Leu(GAG)}$ to a single-site binding model using MicroCal PEAQ-ITC analysis software, we determined that SAM bound to *Pa*TrmD with a K_d of 14.4 ± 3.1 μM and $tRNA^{Leu(GAG)}$ bound to *Pa*TrmD with a similar K_d of 13.6 ± 3.0 μM (Fig. 7). Interestingly the stoichiometry of the *Pa*TrmD:$tRNA^{Leu(GAG)}$ complex was 2:1, which is in line with a published structural study showing that only one of the two possible tRNA binding sites is used at a time on the dimeric TrmD protein (Sakaguchi et al. 2014). The observed binding affinity for SAM and tRNA can be interpreted in light of the estimated concentrations of these ligands in vivo. For example, the intracellular concentration of SAM in *E. coli* is estimated to be ~180 μM (Bennett et al. 2009), while the intracellular concentration of total tRNA in *E. coli* is ~290 μM (Zucconi and Beatty 1988). If each tRNA is assumed to be present at the same concentration, then *Pa*TrmD substrates (nine of 61 tRNAs in PA14 as there are two copies of $tRNA^{Leu(GAG)}$ and $tRNA^{His(GUG)}$) represent ~15% of total tRNA or ~43 μM. Based on this information, it is anticipated that *Pa*TrmD is at least partially bound with tRNA and probably fully bound with SAM (Bennett et al. 2009). However, care must be taken in interpreting these binding results since we have not accounted for confounders such as accessory proteins that might modulate the affinity of *Pa*TrmD binding to specific tRNAs and the effects of other modified ribonucleosides on the affinity of tRNA for *Pa*TrmD.

Sinefungin inhibition and the order of substrate binding to *Pa*TrmD

Results from the steady-state kinetics analyses indicated that both SAM and tRNA must form a ternary complex of *Pa*TrmD:SAM:tRNA in order for the reaction to proceed, while the thermodynamics studies using ITC revealed a similar affinity for tRNA and SAM. However, these results did not give information about the binding order of SAM and tRNA to *Pa*TrmD. To address this problem, we used SFG as a dead-end inhibitor to explore the *Pa*TrmD kinetic mechanism (Fig. 8). The results showed that SFG inhibited

TABLE 3. Steady-state kinetic parameters of *Pa*TrmD

Substrate	K_m (μM)	K_{cat} (min^{-1})	K_{cat}/K_m (min^{-1} μM^{-1})
SAM	3.0 ± 0.8	13.0 ± 1.4	5.3 ± 1.3
$tRNA^{Leu(GAG)}$	0.8 ± 0.2	13.0 ± 1.4	16.0 ± 3.0

The data represent mean ± SD for three independent determinations.

*Pa*TrmD competitively with respect to SAM (Fig. 8A) and uncompetitively with respect to $tRNA^{Leu(GAG)}$ (Fig. 8B). The K_i of SFG with respect to SAM and tRNA were determined as 0.41 ± 0.07 μM and 6.4 ± 0.8 μM, respectively. Based on these results, there are two models—random and ordered—that explain a ternary-complex mechanism for *Pa*TrmD. Interestingly, the binding order of substrates appears to vary among *Pa*TrmD, *Ec*TrmD (Redlak et al. 1997; Brulé et al. 2004), and *Hi*TrmD (Ito et al. 2015; Christian et al. 2016). Studies using product inhibition analysis suggested that *Ec*TrmD uses a random-order binding mechanism, whereas structural studies of *Hi*TrmD suggested a compulsory-order binding mechanism in which SAM binds first followed by tRNA (Ito et al. 2015; Christian et al. 2016). We cannot completely rule out the possibility that these variations may arise from methodological differences. Here a simple comparison of the putative cellular concentrations of SAM 180 μM (Bennett et al. 2009) with the dissociation constant of the complex (14.4 μM, Fig. 7A) indicate that most of *Pa*TrmD molecules in vivo are preloaded with SAM, thus favoring a sequential model where tRNA binds to this preformed binary complex, leading to further structural rearrangements, as suggested in Figure 4 and proposed by Ito et al. (2015). The results of our studies with *Pa*TrmD reveal novel features of this tRNA-modifying enzyme that may explain its unique sensitivity to SAM-competitive inhibitors (Hill et al. 2013).

In summary, we present structural, biochemical, and enzymatic analyses of *Pa*TrmD, which is an essential enzyme for the growth of *P. aeruginosa*. These data give insight into the catalytic mechanism of *Pa*TrmD and should inform antibiotic discovery against this microorganism. The structure of *Pa*TrmD is well conserved with the *Ec*TrmD and *Hi*TrmD further supporting TrmD as a good candidate for the development of broad-spectrum antibiotics targeting microorganisms possessing TrmD. To a large extent, the catalytic mechanism of most SAM-dependent methyltransferases requires no metal as a cofactor. However, bacterial TrmD proteins require Mg^{2+} ions for promoting the methyl transfer reaction. Here we show that an Mg^{2+} ion binds *Pa*TrmD at 1:1 ratio lending further support for the requirement of Mg^{2+} ions for TrmD catalytic activity. Our kinetics data indicate a formation of the ternary complex of *Pa*TrmD:SAM:tRNA in order for the reaction to proceed. The kinetic study using a dead-end inhibitor SFG together with the known cellular concentration of SAM and the fact that *Pa*TrmD was preloaded with SAM in vivo support the binding order of SAM and then tRNA. Our structural data also show the conformational change in the interdomain region, which indicates that the binding of tRNA (likely after SAM binding) induces this change before catalysis can proceed. With regards to substrates of TrmD, G36G37-containing $tRNA^{His}$ is shown in this study as a new tRNA substrate of TrmD in addition to the known substrates $tRNA^{Leu}$, $tRNA^{Pro}$, and $tRNA^{Arg}$.

MATERIALS AND METHODS

Chemicals and reagents

Unless otherwise specified, all chemicals were purchased from Sigma-Aldrich Corporation and used as provided. Single-stranded oligonucleotides and PCR primers were purchased from Integrated DNA Technologies (IDT). Solutions of UltraPure 1 M Tris-HCl, pH 7.5, and molecular biology grade $MgCl_2$ (1 M) for enzyme assays were purchased from ThermoFisher Scientific and Invitrogen, respectively. Methyltransferase-Glo assay kits with *S*-adenosyl-L-methionine (SAM) and *S*-adenosyl-L-homocysteine (SAH) were purchased from Promega.

Construction of TrmD conditional knockout strain (PA1415990::Gm/pBBR-trmD-mSF^{ts1})

The forward and reverse primers (BT4298/BT4299) (Supplemental Table S1) were designed and used to amplify the full-length *trmD* gene (*PA14_15990*) from PA14 genomic

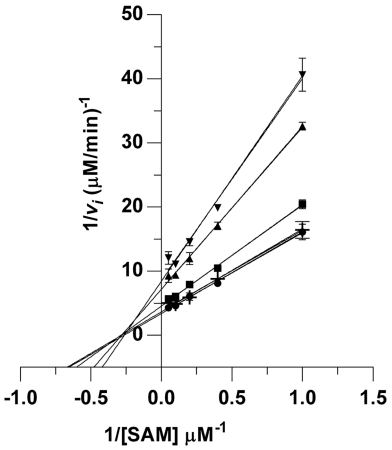

FIGURE 6. Analysis of steady-state kinetics of *Pa*TrmD reveals a ternary complex mechanism. The in vitro *Pa*TrmD assay was used to determine initial velocity (v_i) as a function of SAM and tRNA concentrations. The data were then subjected to a double-reciprocal plot for v_i determined at SAM concentrations ranging over 1–20 μM with different concentrations of $tRNA^{Leu(GAG)}$: 0.4 μM (▼), 0.8 μM (▲), 1.6 μM (■), 3.2 μM (●), or 5 μM (◆). Data points represent mean ± SD for $n = 3$. The intersecting lines suggest that a ternary complex is required for the enzymatic reaction.

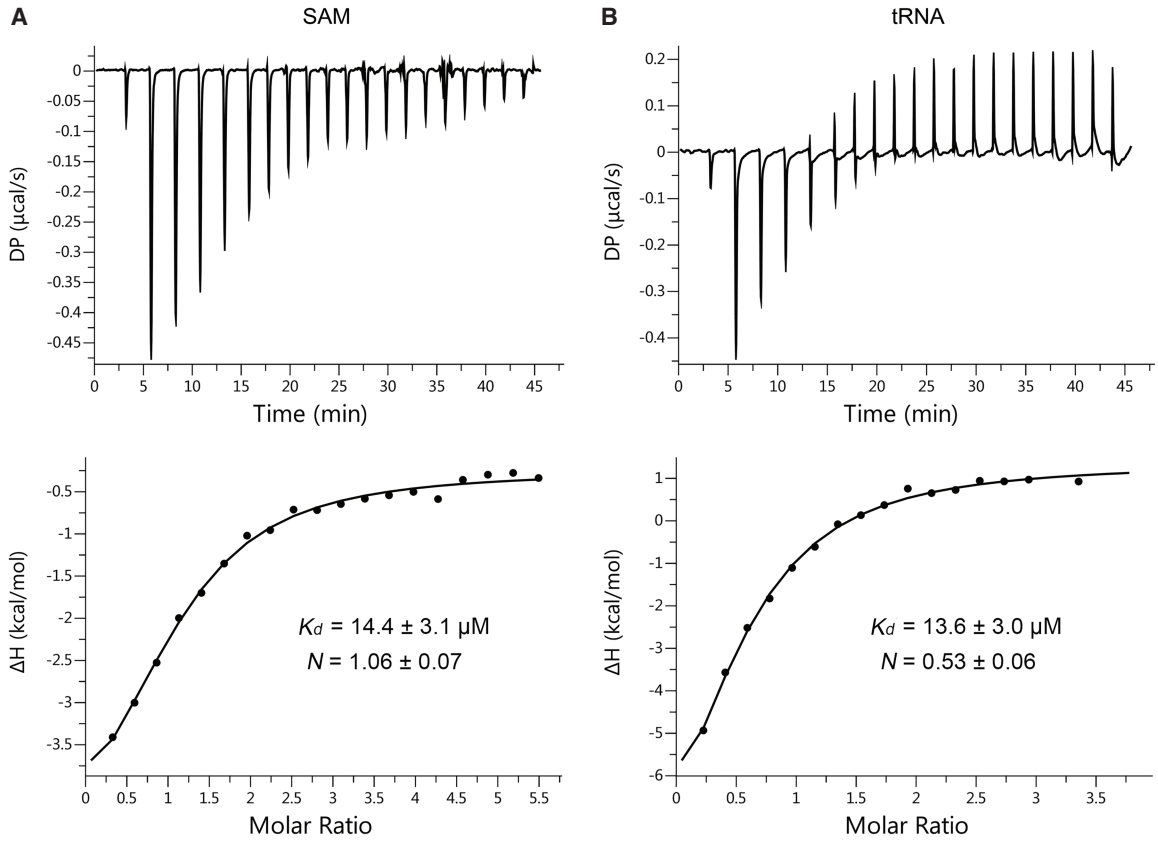

FIGURE 7. Analysis of binding thermodynamics reveals independent binding of SAM and tRNA to *Pa*TrmD. The binding of SAM (*A*) or $tRNA^{Leu(GAG)}$ (*B*) to *Pa*TrmD was quantified by changes in the heat. Data were fit to a single-site fitting model using MicroCal PEAQ-ITC analysis software to determine binding constants (K_d).

DNA and the resulting PCR product was cloned into pBBR1-MCS4 (Kovach et al. 1995) at the SmaI site, yielding the complementation plasmid designated pBBR-*trmD*. To create a temperature-sensitive *trmD* expression plasmid (pBBR-*trmD*-mSF^{ts1}), the fragment containing a temperature-sensitive allele of a *Pseudomonas* replicon, mSF^{ts1}, was obtained from plasmid pSS255 (Silo-Suh et al. 2009) by enzymatic digestion with BamHI, with the resulting digestion fragment cloned into the pBBR-*trmD* plasmid at the BamHI site. The pBBR-*trmD*-mSF^{ts1} plasmid was introduced into *P. aeruginosa* PA14 wild-type strain by electroporation. *P. aeruginosa* PA14 wild-type containing pBBR-*trmD*-mSF^{ts1} was selected on a lysogeny agar plate containing 200 µg mL^{-1} carbenicillin, with the presence of pBBR-*trmD*-mSF^{ts1} verified by PCR analysis. This strain was used as an intermediate in the construction of a *trmD* conditional knockout strain. The upstream and downstream regions of *PA14_15990* were PCR-amplified with the primer pairs BT4316/BT4317 and BT4318/BT4319, respectively, and then cloned into pKNOCK-Ap, a suicide plasmid (Alexeyev 1999) containing a Gm cassette. A pKNOCK-Ap plasmid containing a Gm cassette flanked with upstream (500 bp) and downstream (500 bp) regions of *PA14_15990* (*trmD)* was then transferred into the intermediate strain by conjugation. The transconjugants harboring the allelic exchange of chromosomal *trmD* with a Gm cassette were selected on a lysogeny agar plate containing 75 µg L^{-1} gentamycin. The *Pa*TrmD conditional knockout strain (*trmD*::Gm/pBBR-*trmD*-mSF^{ts1}) was subsequently screened by colony PCR, and confirmed by Southern blot analysis.

Protein expression, purification, crystallization, and data collection

*Pa*TrmD (construct VC008, obtained from NTU Protein Production Platform) spanning residues Leu5 to Asp250, with amino-terminal hexa-histidine tag followed by a TEV cleavage site, was used for crystallization, enzymatic, and kinetics analysis. *E. coli* BL21 (DE3) Rosetta T1R cells harboring *Pa*TrmD plasmid, were cultivated at 37°C to $OD_{600} \sim 1$. The proteins were overexpressed with 0.5 mM IPTG at 18°C for 18 h. Cells were pelleted and stored at −80°C. With all steps performed at 4°C, protein purification was achieved by resuspending thawed pellets in 30 mL of lysis buffer (20 mM Na-HEPES, pH 7.5, 0.3 M NaCl, 10% glycerol, 0.5 mM TCEP), sonicating the pellets in the presence of protease inhibitor cocktail (product 539134, Calbiochem), and clearing the lysates by centrifugation at 58,000*g* for 30 min. The proteins were first purified by affinity chromatography (Ni-NTA agarose, ThermoFisher Scientific), followed by size exclusion chromatography (HiLoad 16/60 Superdex 200, GE Healthcare). The *Pa*TrmD proteins (30,296 Da monomer) eluted as dimers during size exclusion purification. *Pa*TrmD was concentrated to 20 mg mL^{-1} in 20 mM Na-HEPES, pH 7.5, 0.3 M NaCl, 5% (v/v)

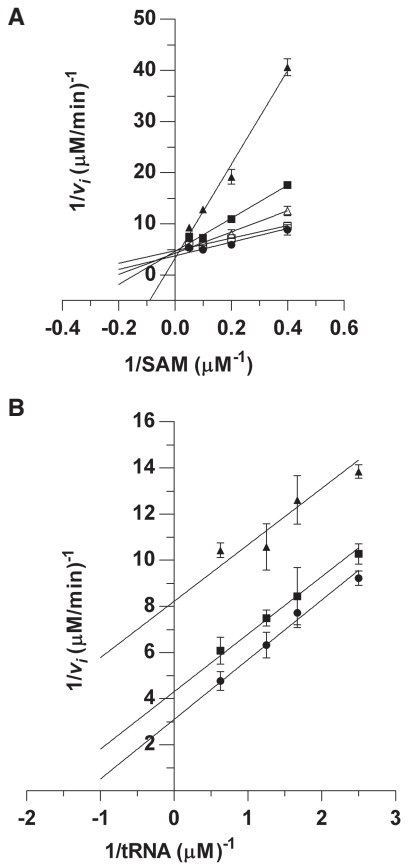

FIGURE 8. Sinefungin inhibition kinetics is consistent with initial binding by tRNA. Dead-end inhibition by SFG was used to assess the order of binding of tRNA and SAM from double-reciprocal plots for the inhibition of methylation by *Pa*TrmD. (*A*) Inhibition by SFG at 0 μM (●), 0.1 μM (■), 0.3 μM (▲), 1 μM (+), or 4 μM (▲) as a function of SAM concentrations ranging from 2.5 to 20 μM. $tRNA^{Leu(GAG)}$ was fixed at 5 μM. (*B*) Inhibition by SFG at 0 μM (●), 4 μM (■), or 8 μM (▲) as a function of $tRNA^{Leu(GAG)}$ concentrations ranging from 0.4 to 1.6 μM. The SAM concentration was fixed at 20 μM. Data points represent mean ± SD ($n = 3$).

glycerol, 0.5 mM TCEP. Aliquots were flash-frozen in liquid nitrogen and stored at −80°C.

An automated initial crystallization screening was performed using the Phoenix crystallization robot (Art Robbins Instruments) at 20°C. Three precipitant: protein ratios (1:1, 1:2 and 2:1) were tested using the vapor diffusion method and commercial crystallization screens (Molecular Dimensions) in Intelli 96-3 wells sitting drop plates. Optimized elongated *Pa*TrmD-SAM crystals were obtained by mixing equal volumes of protein and a precipitant solution containing 0.1 M Tris-HCl, pH 8.4, 12.5% (v/v) MPD, 12.5% (w/v) PEG 1000, 12.5% (w/v) PEG 3350, and 5% (w/v) PEG 200. Prior to data collection, crystals were cryo-protected by a brief soak in the precipitating solution supplemented with 20% (v/v) glycerol and rapidly frozen in liquid nitrogen. The *Pa*TrmD-sinefungin crystals were obtained by soaking the *Pa*TrmD-SAM crystals in the precipitating solution supplemented with 2 mM sinefungin at 20°C for 2 h. For the complex with SFG and Mn^{2+}, one crystal of *Pa*TrmD-SAM was soaked in the precipitating solution supplemented with 10% (v/v) glycerol, 2 mM sinefungin, and 5 mM $MnCl_2$ at 20°C for 24 h. The crystal was then rapidly frozen in liquid nitrogen and data were collected at the K absorption edge of Mn^{2+} (Supplemental Fig. S8) at the Soleil synchrotron. Data collection details are given in Table 1.

For the binding assay, the expression of *Pa*TrmD was as described above. However, the thawed pellet was resuspended in 30 mL of denaturing lysis buffer (20 mM Na-HEPES, pH 7.5, 0.5 M NaCl, 10% (v/v) glycerol, 0.5 mM TCEP, 8 M urea). The supernatant was loaded onto a 5 mL IMAC column (resins packed in Econo-Pac chromatography column, precharged with Ni^{2+}). The column was extensively washed with 30 CV of lysis buffer. After washing, the *Pa*TrmD-bound beads were transferred to a dialysis bag, and dialyzed overnight at 4°C against 1 L of dialysis buffer without urea (20 mM Na-HEPES, pH 7.5, 0.5 M NaCl, 10% glycerol, 0.5 mM TCEP). The overnight dialyzed sample was further dialyzed against a new batch of 1 L dialysis buffer for another 8 h at 4°C. The dialyzed sample was then reloaded onto the IMAC Econo-Pac chromatography column and washed with 5 CV of dialysis buffer. Bound *Pa*TrmD protein was eluted by applying 5 CV of elution buffer (20 mM Na-HEPES, pH 7.5, 500 mM NaCl, 500 mM imidazole, 10% glycerol, 0.5 mM TCEP). The purity of each fraction was checked on SDS-PAGE and fractions containing target protein were pooled and concentrated to 5 mL. Concentrated protein was further purified by size exclusion chromatography and the purified protein was then stored as described above.

Structure determination and refinement

Diffraction intensities were integrated with XDS (Kabsch 2010), scaled, merged and truncated with SCALA/TRUNCATE (Collaborative Computational Project 1994). The structures were determined by molecular replacement using BALBES (Collaborative Computational Project 1994) with the structure from *E. coli* (PDB:1P9P) as a search probe (Elkins et al. 2003). A model for the 3D structure of *Pa*TrmD was built iteratively by using COOT (Emsley and Cowtan 2004) and refined using Autobuster (Smart et al. 2012). The geometrical parameters for sinefungin were generated using coordinates 4R8S from the PDB (www.rcsb.org) and program PRODRG (Schüttelkopf and van Aalten 2004). Structure comparison was performed with the DALI server (echidna.biocenter.helsinki.fi/dali_server/start). The quality of the structures was assessed using the MOLPROBITY server (molprobity.biochem.duke.edu) and figures were generated using the Pymol software (Schrodinger). Data collection and structure refinement parameters are summarized in Table 1. The atomic coordinates and structure factors are deposited with the Protein Data Bank under accession codes 5WYQ (*Pa*TrmD-SAM complex), 5WYR (*Pa*TrmD-sinefungin complex), and 6JKI (*Pa*TrmD-sinefungin-Mn complex).

Magnesium-bound TrmD analysis

The level of Mg^{+2} bound to *Pa*TrmD was measured in the purified *Pa*TrmD and the Mg^{2+}-reconstituted *Pa*TrmD. To prepare the Mg^{2+}-reconstituted *Pa*TrmD, 1 mL solution of 100 μM *Pa*TrmD in 20 mM Na-HEPES, pH 7.5 was incubated with 1 mM $MgCl_2$ for 2 h at 25°C. The unbound Mg^{2+} ion was then removed with a PD-10 desalting column, and the protein was eluted with 20 mM Na-HEPES, pH 7.5. The concentration of the protein was

determined using the Bradford assay. The concentration of Mg^{2+} ion in samples was determined using inductively coupled plasma-optical emission spectrometry (ICP-OES). A calibration curve of Mg^{2+} ion (1000 ppm stock in 2% HNO_3) (Perkin-Elmer) at concentration ranges of 0.025 to 2 ppm for ICP-OES was used to calculate the mole of magnesium ion in samples.

Circular dichroism (CD) experiments

To verify the success of the protein refolding, we compared the CD spectra of native *Pa*TrmD and refolded *Pa*TrmD. Proteins were buffer exchanged to the CD buffer containing 20 mM HEPES pH 7.5, 50 mM NaCl, and concentrated to 0.5 mg ml^{-1}. The spectra were recorded in a cell width of 0.2-mm pathlength (121.QS, Hellma) from 195 to 260 nm at 20°C using a spectropolarimeter (Jasco J-810) equipped with a water-cooled Peltier unit. The spectrum from buffer was first recorded for baseline correction. Data were recorded in mdeg, converted as molar epsilon (Θ), and the spectra were superimposed using Prism.

Preparation of tRNA substrates by in vitro transcription

Single-stranded synthetic DNAs coding for *P. aeruginosa* PA14 $tRNA^{Leu(GAG)}$, $tRNA^{Leu(CAG)}$, $tRNA^{Leu(UAG)}$, $tRNA^{His(GUG)}$, $tRNA^{Pro(GGG)}$, $tRNA^{Pro(CGG)}$, $tRNA^{Pro(UGG)}$, and $tRNA^{Glu(UUG)}$ containing a T7 promoter sequence at 5′-end were PCR-amplified with Phusion High-Fidelity DNA polymerase (Thermo Scientific) using primer pairs listed in Supplemental Table S1. PCR products were then used as templates for in vitro transcription with Mega short script (Thermo, Ambion). At the end of the reaction, the DNA template was removed by DNase digestion and the tRNA transcript was purified and quantified as described previously (Jaroensuk et al. 2016).

In vitro tRNA methylation by *Pa*TrmD

The in vitro transcribed tRNA substrates $tRNA^{Leu(GAG)}$, $tRNA^{Leu(CAG)}$, $tRNA^{Leu(UAG)}$, $tRNA^{His(GUG)}$, $tRNA^{Pro(GGG)}$, $tRNA^{Pro(CGG)}$, $tRNA^{Pro(UGG)}$, and $tRNA^{Gln(UUG)}$ were subjected to methylation reactions by incubating the tRNA with 50 µM of SAM and 100 nM *Pa*TrmD in a buffer containing 50 mM Tris-HCl, pH 7.5, and 5 mM $MgCl_2$ at 37°C for 1 h. Reaction products were analyzed for m^1G content by HPLC-coupled mass spectrometry. These enzyme reaction conditions were not optimized for kinetics assays as described below.

Analysis of *Pa*TrmD methylation products by HPLC-coupled tandem quadrupole mass spectrometry

The tRNA transcripts (2 µg) from the in vitro methylation reactions were enzymatically hydrolyzed to ribonucleosides as described previously (Chan et al. 2011; Su et al. 2014; Jaroensuk et al. 2016). The resulting hydrolysate was analyzed by HPLC-coupled mass spectrometry using a Thermo Hypersil GOLD aQ HPLC column (100 × 2.1 mm, 1.9-µm particle size) operated at 25°C at a flow rate of 0.3 mL min^{-1} with the gradient mixture of mobile phase B (0.1% formic acid in acetonitrile) in mobile phase A (0.1% formic acid in water) as follows: 0–15.3 min, 0%; 15.3–18.7 min, 1%; 18.7–20 min, 6%; 20–27.3 min, 100%; 27.3–41 min, 0%. The HPLC column was directly coupled to an Agilent 6460 triple quadrupole mass spectrometer (LC-MS/MS) with an electrospray ionization source operated in a positive ion mode and the following parameters: gas temperature, 300°C; gas flow, 5 L min^{-1}; nebulizer, 40 psi; sheath gas flow, 7 L min^{-1}; capillary voltage, 3500 V; and dwell time, 100 msec. The mass spectrometer was operated in multiple reaction monitoring (MRM) mode to detect and quantify a variety of potential methylation products based on retention time, *m/z* of the transmitted parent ion, *m/z* of the monitored product, fragmentor voltages, and collision energy as noted in Supplemental Table S2. The identities of methylation products were confirmed by comparison with the synthetic standards.

Mapping *Pa*TrmD products in tRNA by HPLC-coupled mass spectrometry

In vitro methylated $tRNA^{Leu(GAG)}$ transcript (5 µg) were digested with 5 U of RNase A and dephosphorylated with 10 U of bacterial alkaline phosphatase in 10 mM ammonium acetate buffer (pH 7.0) at 37°C for 4 h in the presence of deaminase inhibitors and antioxidants as described previously (Chan et al. 2011; Su et al. 2014; Jaroensuk et al. 2016). The RNA fragments were then resolved by HPLC using an Amide-HILIC TSK-gel Amide-80 column (2.0 mm ID × 150 mm, 3 µm particle size) coupled to a quadrupole time-of-flight mass spectrometer (Agilent 6520) with an electrospray ionization source operated in a negative ion mode as described previously (Chionh et al. 2016). Collision-induced dissociation (CID) analysis was performed to obtain sequence information from the RNase A-digested products. Collision energies were varied from 25 to 40 V and products were scanned from *m/z* 100 to 2000, with RNA sequences determined using a-B, w and y ions.

Developing an in vitro *Pa*TrmD assay for kinetics studies

For the kinetics assays, we developed an in vitro assay for *Pa*TrmD activity based on the MTase-Glo coupled bioluminescent assay. In this assay, the SAH that is a product of the *Pa*TrmD methylation reaction with SAM is converted to ADP by coupling enzymes in the MTase-Glo reagent. ADP is then converted to ATP using MTase-Glo detection solution generating a luminescent signal, which is proportional to the TrmD methyltransferase activity. We optimized the *Pa*TrmD concentration by varying it from 0 to 100 nM. Reactions were prepared in 50 mM Tris-HCl pH 7.5, 5 mM $MgCl_2$, 4 µM synthetic $tRNA^{Leu(GAG)}$, 50 µM SAM, and 1× MTase-Glo reagent in a final volume of 55 µL. The reaction was incubated at 37°C for 5 min and a 10 µL aliquot was removed for the zero time point (T_0). *Pa*TrmD (1 µL) was then added to initiate the reaction. During the 8-min time course at 37°C, 10 µL aliquots were collected every 2 min and quenched with 10 µL of MTase-Glo detection solution prepared in a 384-well plate (Grenier Item No. 784904; white color). The plate was incubated at ambient temperature for 30 min and the luminescence signal was quantified using a luminometer plate reader (Thermo Scientific). The resulting luminescent signal was then converted to SAH concentration using the SAH standard curve. A reaction

without *Pa*TrmD was performed as a control. The initial velocities (v_i) were determined by plotting the SAH concentration as a function of time and the data were fitted by linear regression with GraphPad Prism version 6 (GraphPad Software, Inc.).

Determination of two-substrate *Pa*TrmD steady-state kinetics

The steady-state kinetics parameters for *Pa*TrmD were determined using the MTase-Glo assay (Hsiao et al. 2016) described earlier with varying concentrations of $tRNA^{Leu(GAG)}$ (0.4–5.0 μM) or SAM (1–20 μM) and the *Pa*TrmD concentration fixed at 23 nM. Reactions were initiated by adding *Pa*TrmD and monitored using a luminometer plate reader (Thermo Scientific). The initial velocities (v) were measured as described above. The methylation kinetic parameters of the *Pa*TrmD reaction were determined by plotting initial velocities versus substrate concentrations as described by a ternary-complex rate Equation 1, where A is SAM, B is $tRNALeu^{GAG}$, K_a and K_b are the Michaelis constants for substrate A and B, respectively, and K'_a is the dissociation constant for enzyme-SAM complex. Data were fitted to the equation using GraphPad Prism version 6 (GraphPad Software, Inc.) and GraFit version 7 (Erithacus Software, Ltd.) for global analysis.

$$v = \frac{V_{max}[A][B]}{K'_a K_b + K_b[A] + K_a[B] + [A][B]} \quad (1)$$

Isothermal titration calorimetry (ITC) assay

Assessment of SAM and tRNA binding to refolded *Pa*TrmD was performed with a MicroCal PEAQ-ITC (Malvern Instruments Limited). The refolded *Pa*TrmD and tRNA used for the experiments were dialyzed extensively against a buffer comprised of 50 mM Na-HEPES, pH7.5, 5 mM $MgCl_2$, and the dialysate was used to prepare fresh working solutions of SAM. Titrations were performed at 25°C and consisted of a single initial injection of 0.5 μL, followed by 19 injections of 2 μL of either 800 μM SAM or 550 μM of tRNA into the sample cell containing 30 μM refolded *Pa*TrmD. Two consecutive injections were separated by 3 min to allow the binding to come to equilibrium. Thermodynamic data were analyzed with a single-site fitting model using MicroCal PEAQ-ITC analysis software provided by the manufacturer.

Sinefungin (SFG) inhibition study

Inhibition of *Pa*TrmD by the SAM substrate analog sinefungin (SFG) was investigated by measuring reaction velocities at fixed concentrations of SAM and tRNA with varying concentrations of sinefungin (0, 0.1, 0.3, 1, or 4 μM). Reactions were performed in 50 mM Tris-HCl pH 7.5, 5 mM $MgCl_2$, 1× MTase-Glo reagent, a saturating concentration of $tRNA^{Leu(GAG)}$ (5 μM), *Pa*TrmD at 23 nM and various concentrations of SAM (2.5–20 μM). Assays were initiated by adding *Pa*TrmD and the residual activity of *Pa*TrmD in the presence of varying SFG concentrations was measured. The double-reciprocal plot of initial velocities (v) and SAM at various concentrations of SFG was plotted and the inhibition constant (K_i) for sinefungin with respect to SAM was determined by a competitive inhibition equation (Equation 2), where V_{max} is the maximum velocity of enzyme reaction, [S] is the SAM concentration, K_m is the Michaelis constant for SAM, [I] is the SFG concentration and K_i is the inhibition constant for competitive inhibition. Data were fitted to Equation 2 using a GraphPad Prism version 6 (GraphPad Software, Inc.).

$$v = \frac{V_{max}[S]}{K_m(1 + [I]/K_i) + [S]} \quad (2)$$

Analysis of SFG inhibition with respect to tRNA concentration was also performed and carried out as described above, except that the SAM concentration was kept constant at 20 μM while the tRNA concentrations were varied from 0.4 to 1.6 μM. *Pa*TrmD activity was measured in the presence of SFG concentrations of 0, 4 and 8 μM. The double-reciprocal plot of the initial velocities and tRNA concentrations was analyzed and the K_i for SFG with respect to tRNA was determined using an uncompetitive inhibition equation (Equation 3), where V_{max} is the maximum velocity of enzyme reaction, [S] is a tRNA concentration, K_m is the Michaelis constant for tRNA, [I] is an SFG concentration, and K_i is the inhibition constant for uncompetitive inhibition. Data were fitted to Equation 3 using GraphPad Prism version 6 (GraphPad Software, Inc.).

$$v = \frac{V_{max}[S]/(1 + [I]/K_i)}{K_m(1 + [I]/K_i) + [S]} \quad (3)$$

DATA DEPOSITION

Atomic coordinates and structure factors for the reported crystal structures have been deposited with the Protein Data bank under accession numbers 5WYQ, 5WYR, and 6JKI.

SUPPLEMENTAL MATERIAL

Supplemental material is available for this article.

ACKNOWLEDGMENTS

The authors wish to thank Dr. Amnart Khongmanee and Mr. Bhawat Wongkhamprai for technical assistance with QTOF analysis, Mr. Pin Koon Ee for technical assistance with in vitro transcription of tRNA, Professor M.R. Jisnuson Svasti, Dr. Paiboon Vattanaviboon, Dr. Nisanart Charoenlap, and Dr. Nilubol Paricharttanakul for discussion of enzyme kinetics, and scientists from Swiss Light Source for their help with diffraction data collection. This work was supported by the Chulabhorn Graduate Institute (ABS-02 to M.F.); by the National Research Foundation of Singapore under its Singapore-MIT Alliance for Research and Technology Infectious Disease and Antimicrobial Resistance Interdisciplinary Research Groups (P.C.D. and J.L.); by the US National Science Foundation (CHE-1308839 to P.C.D.); by the SMART Innovation Centre (ING137070-BIO to P.C.D. and J.L.); and by the Thailand Research Fund (5980001 to P.C.).

Received June 9, 2018; accepted July 28, 2019.

REFERENCES

Ahn HJ, Kim HW, Yoon HJ, Lee BI, Suh SW, Yang JK. 2003. Crystal structure of tRNA(m^1G37)methyltransferase: insights into tRNA recognition. *EMBO J* **22:** 2593–2603. doi:10.1093/emboj/cdg269

Alexeyev MF. 1999. The pKNOCK series of broad-host-range mobilizable suicide vectors for gene knockout and targeted DNA insertion into the chromosome of gram-negative bacteria. *BioTechniques* **26:** 824–826, 828. doi:10.2144/99265bm05

Baumgartner MP, Camacho CJ. 2016. Choosing the optimal rigid receptor for docking and scoring in the CSAR 2013/2014 experiment. *J Chem Inf Model* **56:** 1004–1012. doi:10.1021/acs.jcim.5b00338

Begley U, Dyavaiah M, Patil A, Rooney JP, DiRenzo D, Young CM, Conklin DS, Zitomer RS, Begley TJ. 2007. Trm9-catalyzed tRNA modifications link translation to the DNA damage response. *Mol Cell* **28:** 860–870. doi:10.1016/j.molcel.2007.09.021

Bennett BD, Kimball EH, Gao M, Osterhout R, Van Dien SJ, Rabinowitz JD. 2009. Absolute metabolite concentrations and implied enzyme active site occupancy in *Escherichia coli*. *Nat Chem Biol* **5:** 593–599. doi:10.1038/nchembio.186

Björk GR, Nilsson K. 2003. 1-methylguanosine-deficient tRNA of *Salmonella enterica* serovar Typhimurium affects thiamine metabolism. *J Bacteriol* **185:** 750–759. doi:10.1128/JB.185.3.750-759.2003

Björk GR, Wikström PM, Byström AS. 1989. Prevention of translational frameshifting by the modified nucleoside 1-methylguanosine. *Science (80-)* **244:** 986–989. doi:10.1126/science.2471265

Björk GR, Jacobsson K, Nilsson K, Johansson MJ, Byström AS, Persson OP. 2001. A primordial tRNA modification required for the evolution of life? *EMBO J* **20:** 231–239. doi:10.1093/emboj/20.1.231

Brulé H, Elliott M, Redlak M, Zehner ZE, Holmes WM. 2004. Isolation and characterization of the human tRNA-(N^1G37) methyltransferase (TRM5) and comparison to the *Escherichia coli* TrmD protein. *Biochemistry* **43:** 9243–9255. doi:10.1021/bi049671q

Byström AS, Björk GR. 1982. Chromosomal location and cloning of the gene (*trmD*) responsible for the synthesis of tRNA (m^1G) methyltransferase in *Escherichia coli* K-12. *Mol Gen Genet* **188:** 440–446. doi:10.1007/BF00330046

Centers for Disease Control Ministry of Health and Welfare R.O.C. (Taiwan). 2010. Statistics of communicable diseases and surveillance report: nosocomial infections surveillance system. In *Statistics of communicable diseases and surveillance report: nosocomial infections surveillance system*. Centers for Disease Control, Ministry of Health and Welfare, R.O.C. (Taiwan).

Chan PP, Lowe TM. 2016. GtRNAdb 2.0: an expanded database of transfer RNA genes identified in complete and draft genomes. *Nucleic Acids Res* **44:** D184–D189. doi:10.1093/nar/gkv1309

Chan CT, Chionh YH, Ho CH, Lim KS, Babu IR, Ang E, Wenwei L, Alonso S, Dedon PC. 2011. Identification of N^6,N^6-dimethyladenosine in transfer RNA from *Mycobacterium bovis* Bacille Calmette-Guerin. *Molecules* **16:** 5168–5181. doi:10.3390/molecules16065168

Chan CT, Pang YL, Deng W, Babu IR, Dyavaiah M, Begley TJ, Dedon PC. 2012. Reprogramming of tRNA modifications controls the oxidative stress response by codon-biased translation of proteins. *Nat Commun* **3:** 937. doi:10.1038/ncomms1938

Chaudhuri RR, Allen AG, Owen PJ, Shalom G, Stone K, Harrison M, Burgis TA, Lockyer M, Garcia-Lara J, Foster SJ, et al. 2009. Comprehensive identification of essential *Staphylococcus aureus* genes using transposon-mediated differential hybridisation (TMDH). *BMC Genomics* **10:** 291. doi:10.1186/1471-2164-10-291

Chionh YH, McBee M, Babu IR, Hia F, Lin W, Zhao W, Cao J, Dziergowska A, Malkiewicz A, Begley TJ, et al. 2016. tRNA-mediated codon-biased translation in mycobacterial hypoxic persistence. *Nat Commun* **7:** 13302. doi:10.1038/ncomms13302

Christian T, Hou YM. 2007. Distinct determinants of tRNA recognition by the TrmD and Trm5 methyl transferases. *J Mol Biol* **373:** 623–632. doi:10.1016/j.jmb.2007.08.010

Christian T, Sakaguchi R, Perlinska AP, Lahoud G, Ito T, Taylor EA, Yokoyama S, Sulkowska JI, Hou YM. 2016. Methyl transfer by substrate signaling from a knotted protein fold. *Nat Struct Mol Biol* **23:** 941–948. doi:10.1038/nsmb.3282

Collaborative Computational Project, Number 4. 1994. The CCP4 suite: programs for protein crystallography. *Acta Crystallogr D Biol Crystallogr* **50:** 760–763. doi:10.1107/S0907444994003112

de Berardinis V, Vallenet D, Castelli V, Besnard M, Pinet A, Cruaud C, Samair S, Lechaplais C, Gyapay G, Richez C, et al. 2008. A complete collection of single-gene deletion mutants of *Acinetobacter baylyi* ADP1. *Mol Syst Biol* **4:** 174. doi:10.1038/msb.2008.10

Elkins PA, Watts JM, Zalacain M, van Thiel A, Vitazka PR, Redlak M, Andraos-Selim C, Rastinejad F, Holmes WM. 2003. Insights into catalysis by a knotted TrmD tRNA methyltransferase. *J Mol Biol* **333:** 931–949. doi:10.1016/j.jmb.2003.09.011

El Yacoubi B, Bailly M, de Crécy-Lagard V. 2012. Biosynthesis and function of posttranscriptional modifications of transfer RNAs. *Annu Rev Genet* **46:** 69–95. doi:10.1146/annurev-genet-110711-155641

Emsley P, Cowtan K. 2004. *Coot*: model-building tools for molecular graphics. *Acta Crystallogr D Biol Crystallogr* **60:** 2126–2132. doi:10.1107/S0907444904019158

Forsyth RA, Haselbeck RJ, Ohlsen KL, Yamamoto RT, Xu H, Trawick JD, Wall D, Wang L, Brown-Driver V, Froelich JM, et al. 2002. A genome-wide strategy for the identification of essential genes in *Staphylococcus aureus*. *Mol Microbiol* **43:** 1387–1400. doi:10.1046/j.1365-2958.2002.02832.x

Goto-Ito S, Ito T, Ishii R, Muto Y, Bessho Y, Yokoyama S. 2008. Crystal structure of archaeal tRNA(m^1G37)methyltransferase aTrm5. *Proteins* **72:** 1274–1289. doi:10.1002/prot.22019

Hagervall TG, Tuohy TM, Atkins JF, Björk GR. 1993. Deficiency of 1-methylguanosine in tRNA from *Salmonella typhimurium* induces frameshifting by quadruplet translocation. *J Mol Biol* **232:** 756–765. doi:10.1006/jmbi.1993.1429

Hill PJ, Abibi A, Albert R, Andrews B, Gagnon MM, Gao N, Grebe T, Hajec LI, Huang J, Livchak S, et al. 2013. Selective inhibitors of bacterial t-RNA-(N^1G37) methyltransferase (TrmD) that demonstrate novel ordering of the lid domain. *J Med Chem* **56:** 7278–7288. doi:10.1021/jm400718n

Hjalmarsson KJ, Byström AS, Björk GR. 1983. Purification and characterization of transfer RNA (guanine-1)methyltransferase from *Escherichia coli*. *J Biol Chem* **258:** 1343–1351.

Hong DJ, Bae IK, Jang IH, Jeong SH, Kang HK, Lee K. 2015. Epidemiology and characteristics of metallo-β-lactamase-producing *Pseudomonas aeruginosa*. *Infect Chemother* **47:** 81–97. doi:10.3947/ic.2015.47.2.81

Hou YM, Matsubara R, Takase R, Masuda I, Sulkowska JI. 2017. TrmD: a methyl transferase for tRNA methylation with m^1G37. *Enzymes* **41:** 89–115. doi:10.1016/bs.enz.2017.03.003

Hsiao K, Zegzouti H, Goueli SA. 2016. Methyltransferase-Glo: a universal, bioluminescent and homogenous assay for monitoring all classes of methyltransferases. *Epigenomics* **8:** 321–339. doi:10.2217/epi.15.113

Ito T, Masuda I, Yoshida K, Goto-Ito S, Sekine S, Suh SW, Hou YM, Yokoyama S. 2015. Structural basis for methyl-donor-dependent and sequence-specific binding to tRNA substrates by knotted methyltransferase TrmD. *Proc Natl Acad Sci* **112:** E4197–4205. doi:10.1073/pnas.1422981112

Jaroensuk J, Atichartpongkul S, Chionh YH, Wong YH, Liew CW, McBee ME, Thongdee N, Prestwich EG, DeMott MS, Mongkolsuk S, et al. 2016. Methylation at position 32 of tRNA catalyzed by TrmJ alters oxidative stress response in *Pseudomonas aeruginosa*. *Nucleic Acids Res* **44:** 10834–10848. doi:10.1093/nar/gkw870

Kabsch W. 2010. Integration, scaling, space-group assignment and post-refinement. *Acta Crystallogr D Biol Crystallogr* **66:** 133–144. doi:10.1107/S0907444909047374

Kovach ME, Elzer PH, Hill DS, Robertson GT, Farris MA, Roop RM II, Peterson KM. 1995. Four new derivatives of the broad-host-range cloning vector pBBR1MCS, carrying different antibiotic-resistance cassettes. *Gene* **166:** 175–176. doi:10.1016/0378-1119(95)00584-1

Lahoud G, Goto-Ito S, Yoshida K, Ito T, Yokoyama S, Hou YM. 2011. Differentiating analogous tRNA methyltransferases by fragments of the methyl donor. *RNA* **17:** 1236–1246. doi:10.1261/rna.2706011

Li JN, Björk GR. 1995. 1-Methylguanosine deficiency of tRNA influences cognate codon interaction and metabolism in *Salmonella typhimurium*. *J Bacteriol* **177:** 6593–6600. doi:10.1128/jb.177.22.6593-6600.1995

Li JN, Björk GR. 1999. Structural alterations of the tRNA(m^1G37)methyltransferase from *Salmonella typhimurium* affect tRNA substrate specificity. *RNA* **5:** 395–408. doi:10.1017/S1355838299980834

Liu J, Wang W, Shin DH, Yokota H, Kim R, Kim SH. 2003. Crystal structure of tRNA (m^1G37) methyltransferase from *Aquifex aeolicus* at 2.6 Å resolution: a novel methyltransferase fold. *Proteins* **53:** 326–328. doi:10.1002/prot.10479

Lucena A, Dalla Costa LM, Nogueira KS, Matos AP, Gales AC, Paganini MC, Castro ME, Raboni SM. 2014. Nosocomial infections with metallo-β-lactamase-producing *Pseudomonas aeruginosa*: molecular epidemiology, risk factors, clinical features and outcomes. *J Hosp Infect* **87:** 234–240. doi:10.1016/j.jhin.2014.05.007

National Nosocomial Infections Surveillance System. 2004. National Nosocomial Infections Surveillance (NNIS) System Report, data summary from January 1992 through June 2004, issued October 2004. *Am J Infect Control* **32:** 470–485. doi:10.1016/j.ajic.2004.10.001

O'Dwyer K, Watts JM, Biswas S, Ambrad J, Barber M, Brulé H, Petit C, Holmes DJ, Zalacain M, Holmes WM. 2004. Characterization of *Streptococcus pneumoniae* TrmD, a tRNA methyltransferase essential for growth. *J Bacteriol* **186:** 2346–2354. doi:10.1128/JB.186.8.2346-2354.2004

Redlak M, Andraos-Selim C, Giege R, Florentz C, Holmes WM. 1997. Interaction of tRNA with tRNA (guanosine-1)methyltransferase: binding specificity determinants involve the dinucleotide $G^{36}pG^{37}$ and tertiary structure. *Biochemistry* **36:** 8699–8709. doi:10.1021/bi9701538

Rozenski J, McCloskey JA. 2002. SOS: a simple interactive program for ab initio oligonucleotide sequencing by mass spectrometry. *J Am Soc Mass Spectrom* **13:** 200–203. doi:10.1016/S1044-0305(01)00354-3

Sakaguchi R, Lahoud G, Christian T, Gamper H, Hou YM. 2014. A divalent metal ion-dependent N^1-methyl transfer to G37-tRNA. *Chem Biol* **21:** 1351–1360. doi:10.1016/j.chembiol.2014.07.023

Schüttelkopf AW, van Aalten DM. 2004. *PRODRG*: a tool for high-throughput crystallography of protein-ligand complexes. *Acta Crystallogr D Biol Crystallogr* **60:** 1355–1363. doi:10.1107/S0907444904011679

Silo-Suh LA, Elmore B, Ohman DE, Suh SJ. 2009. Isolation, characterization, and utilization of a temperature-sensitive allele of a *Pseudomonas* replicon. *J Microbiol Methods* **78:** 319–324. doi:10.1016/j.mimet.2009.07.002

Smart OS, Womack TO, Flensburg C, Keller P, Paciorek W, Sharff A, Vonrhein C, Bricogne G. 2012. Exploiting structure similarity in refinement: automated NCS and target-structure restraints in *BUSTER*. *Acta Crystallogr D Biol Crystallogr* **68:** 368–380. doi:10.1107/S0907444911056058

Sprinzl M, Vassilenko KS. 2005. Compilation of tRNA sequences and sequences of tRNA genes. *Nucleic Acids Res* **33:** D139–140. doi:10.1093/nar/gki012

Su D, Chan CT, Gu C, Lim KS, Chionh YH, McBee ME, Russell BS, Babu IR, Begley TJ, Dedon PC. 2014. Quantitative analysis of ribonucleoside modifications in tRNA by HPLC-coupled mass spectrometry. *Nat Protoc* **9:** 828–841. doi:10.1038/nprot.2014.047

Subramanian M, Srinivasan T, Sudarsanam D. 2014. Examining the Gm18 and m^1G modification positions in tRNA sequences. *Genomics Inform* **12:** 71–75. doi:10.5808/GI.2014.12.2.71

Takeda H, Toyooka T, Ikeuchi Y, Yokobori S, Okadome K, Takano F, Oshima T, Suzuki T, Endo Y, Hori H. 2006. The substrate specificity of tRNA (m^1G37) methyltransferase (TrmD) from *Aquifex aeolicus*. *Genes Cells* **11:** 1353–1365. doi:10.1111/j.1365-2443.2006.01022.x

Taylor DE, Trieber CA, Trescher G, Bekkering M. 1998. Host mutations (*miaA* and *rpsL*) reduce tetracycline resistance mediated by Tet(O) and Tet(M). *Antimicrob Agents Chemother* **42:** 59–64. doi:10.1128/AAC.42.1.59

Ventola CL. 2015. The antibiotic resistance crisis: part 1: causes and threats. *P T* **40:** 277–283.

Winsor GL, Lam DK, Fleming L, Lo R, Whiteside MD, Yu NY, Hancock RE, Brinkman FS. 2011. Pseudomonas Genome Database: improved comparative analysis and population genomics capability for *Pseudomonas* genomes. *Nucleic Acids Res* **39:** D596–D600. doi:10.1093/nar/gkq869

Zucconi AP, Beatty JT. 1988. Posttranscriptional regulation by light of the steady-state levels of mature B800-850 light-harvesting complexes in *Rhodobacter capsulatus*. *J Bacteriol* **170:** 877–882. doi:10.1128/jb.170.2.877-882.1988